# Photocatalytic Hydroxylation of Benzene by Dioxygen to Phenol with a Cyano-Bridged Complex Containing Fe^II and Ru^II Incorporated in Mesoporous Silica–Alumina

# Photocatalytic Hydroxylation of Benzene by Dioxygen to Phenol with a Cyano-Bridged Complex Containing $Fe^{II}$ and $Ru^{II}$ Incorporated in Mesoporous Silica–Alumina

Yusuke Aratani, Kohei Oyama, Tomoyoshi Suenobu, Yusuke Yamada and Shunichi Fukuzumi

# Photocatalytic Hydroxylation of Benzene by Dioxygen to Phenol with a Cyano-Bridged Complex Containing $Fe^{II}$ and $Ru^{II}$ Incorporated in Mesoporous Silica-Alumina

*Yusuke Aratani,*[†] *Kohei Oyama,* [†] *Tomoyoshi Suenobu,*[†] *Yusuke Yamada,**[,‡] *and Shunichi Fukuzumi**[,†,§,||]

[†]Department of Material and Life Science, Graduate School of Engineering, Osaka University, ALCA and SENTAN, Japan Science and Technology Agency (JST), Suita, Osaka 565-0871, Japan

[‡]Department of Applied Chemistry and Bioengineering, Graduate School of Engineering, Osaka City University, Osaka 558-8585, Japan

[§]Department of Chemistry and Nano Science, Ewha Womans University, Seoul 120-750, Korea

[||]Faculty of Science and Engineering, Meijo University, ALCA and SENTAN, Japan Science and Technology Agency (JST), Nagoya, Aichi 468-0073, Japan

**Abstract:** Photocatalytic hydroxylation of benzene to phenol has been achieved by using $O_2$ as an oxidant as well as an oxygen source with a cyano-bridged polynuclear metal complex containing $Fe^{II}$ and $Ru^{II}$ incorporated in mesoporous silica-alumina ($[Fe(H_2O)_3]_2[Ru(CN)_6]$@sAl-MCM-41). An apparent turnover number (TON) of phenol production per the monomer unit of $[Fe(H_2O)_3]_2[Ru(CN)_6]$ was 41 for 59 h. The cyano-bridged polynuclear metal complex, $[Fe(H_2O)_3]_2[Ru(CN)_6]$, exhibited catalytic activity for thermal hydroxylation of benzene by $H_2O_2$ in acetonitrile (MeCN), where the apparent TON of phenol production reached 393 for 60 h. The apparent TON increased to 2500 for 114 h by incorporating $[Fe(H_2O)_3]_2[Ru(CN)_6]$ in sAl-MCM-41. Additionally, $[Fe(H_2O)_3]_2[Ru(CN)_6]$ acts as a water oxidation catalyst by using $[Ru(bpy)_3]^{2+}$ (bpy = 2, 2'-bipyridine) and $Na_2S_2O_8$ as a photosensitizer and a sacrificial electron acceptor as evidenced by $^{18}O$-isotope labeling experiments. Photoirradiation of an $O_2$-saturated MeCN solution containing $[Fe(H_2O)_3]_2[Ru(CN)_6]$@sAl-MCM-41 and scandium ion provided $H_2O_2$ formation, where photoexcited $[Ru(CN)_6]^{4-}$ moiety reduces $O_2$ as indicated by laser flash photolysis measurements. Thus, hydroxylation of benzene to phenol using molecular oxygen photocatalyzed by $[Fe(H_2O)_3]_2[Ru(CN)_6]$ occurred via a two-step route; 1) molecular oxygen was photocatalytically reduced to peroxide by using water as an electron donor, and then, 2) peroxide thus formed is used as an oxidant for hydroxylation of benzene.

## Introduction

Production of phenol from benzene in a one-step reaction has merited significant interest from the viewpoints of an environmentally benign green process and economical efficiency as compared with the current three-step cumene process.[1-3] Thus, extensive efforts have so far been devoted to develop the one-step direct hydroxylation of benzene using various oxidants such as $H_2O_2$,[4-7] $N_2O$,[8,9] $O_2$ with reductants.[10-15] Catalytic oxidation of benzene using $O_2$ as the oxidant is particularly of high potential interest, because $O_2$ is regarded as an ideal oxidant due to its natural, inexpensive, and environmentally friendly characteristics. However, catalytic aerobic oxidation of benzene via $O_2$ activation without reductants required harsh reaction conditions such as high temperature and high pressures.[16-19] Photocatalytic oxidation of benzene with $O_2$ without a reductant has also been reported using organic photocatalysts.[20-23] In such a case, water was used as an oxygen source whereas $O_2$ acts only as an oxidant.[20-23] Thus, there has been no report on catalytic hydroxylation of benzene with $O_2$ used as an oxygen source as well as an oxidant under mild conditions at ambient pressure and temperature.

Recently, photocatalytic systems producing $H_2O_2$ by reduction of $O_2$ with water as an electron donor have been constructed by utilizing the water oxidation catalysis of cyano-bridged complexes and $O_2$ reduction catalysis of a Ru complex.[24-26] On the other hand, some metal complexes containing iron ions have been reported to act as a catalyst for hydroxylation of benzene by $H_2O_2$.[27-31] Combination of catalysis for photocatalytic $H_2O_2$ production and for hydroxylation of benzene by $H_2O_2$ allows to construct a composite catalyst for benzene hydroxylation by $O_2$. A cyano-bridged complex incorporating Ru(II) ions and Fe(II) ions seems to be a good candidate for such a reaction.

We report herein photocatalytic hydroxylation of benzene to phenol using $O_2$ as an oxygen source as well as an oxidant with a cyano-bridged polynuclear metal complex containing $Fe^{II}$ and $Ru^{II}$ incorporated in mesoporous silica-alumina ($[Fe(H_2O)_3]_2[Ru(CN)_6]$@sAl-MCM-41), in MeCN under photoirradiation at 298 K. As indicated in Figure 1, Fe ions in $[Fe(H_2O)_3]_2[Ru(CN)_6]$ have extraligands such as water molecules to fulfill octahedral coordination, however, the coordinating water molecules are easily liberated during the catalytic reaction. The $Fe^{II}$ ions may react with $H_2O_2$ to produce hydroxyl radicals or iron oxo species, which oxidize benzene to produce phenol. The incorporated metal complex, $[Fe(H_2O)_3]_2[Ru(CN)_6]$, acts as both an effective photocatalyst for oxidation of water with $O_2$ to produce $H_2O_2$ and also an excellent catalyst for hydroxylation of benzene with $H_2O_2$ to produce phenol.

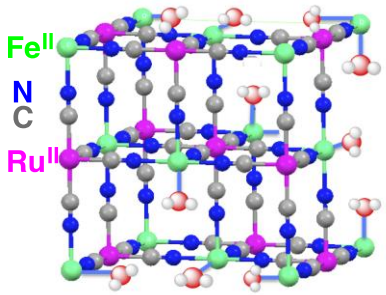


**Figure 1.** Partial structure of a cyano-bridged complex containing $Fe^{II}$ and $Ru^{II}$ ($[Fe(H_2O)_3]_2[Ru(CN)_6]$). Three water molecules (in average) bind to $Fe^{II}$ ions to fulfill the octahedral coordination structure.

## Experimental Section

**Materials.** All chemicals used for synthesis were obtained from chemical companies and used without further purification. Purified water was provided by a water purification system, Millipore Direct-Q3 UV, where the electronic conductance was 18.2 MΩ cm. Tetraethyl

orthosilicate, copper(II) sulfate pentahydrate, cobalt(II) nitrate hexahydrate, manganese(II) perchlorate hexahydrate, cetyltrimethylammonium bromide, sodium aluminate, aqueous ammonia, benzene, sodium iodide and an aqueous solution of hydrogen peroxide (30 wt%) were purchased from Wako Pure Chemical Industries. Iron(II) perchlorate hydrate and potassium hexacyanoruthenate(II) hydrate were delivered by Sigma-Aldrich. Acetonitrile was obtained from Nacalai tesque. Potassium hexacyanorhodate(III) and scandium(III) nitrate was supplied by Mitsuwa Chemicals Co., Ltd.

**Synthesis of $[Mn(H_2O)_3]_2[Ru(CN)_6]$, $[Fe(H_2O)_3]_2[Ru(CN)_6]$, $[Co(H_2O)_3]_2[Ru(CN)_6]$, $[Cu(H_2O)_n]_2[Ru(CN)_6]$.**[32] An aqueous solution (10 mL) of manganese(II) perchlorate hexahydrate, iron(II) perchlorate hydrate, cobalt(II) nitrate hexahydrate or copper(II) sulfate pentahydrate (0.14 mmol) was slowly added to an aqueous solution (10 mL) of potassium hexacyanoruthenate(II) hydrate (0.073 mmol) for 2 h with stirring magnetically. The formed precipitate was collected by filtration, washed with water and dried *in vacuo*.

**Synthesis of $[Fe(H_2O)_2]_{1.5}[Rh(CN)_6]$.**[32] An aqueous solution (10 mL) of iron(II) perchlorate hydrate (0.20 mmol) was slowly added to an aqueous solution (10 mL) of potassium hexacyanorhodate(III) (0.13 mmol) for 2 h with stirring magnetically. The obtained precipitate was collected by filtration, washed with water and dried *in vacuo*.

**Synthesis of Spherical Mesoporous Silica-Alumina (sAl-MCM-41).**[33] sAl-MCM-41 was synthesized by a reported method with modifications.[33] Cetyltrimethylammonium bromide (14.6 g) was dissolved to a mixed solution (814 mL) composed of water, aqueous $NH_3$ and ethanol [270 : 444 : 100 (v/v/v)]. Tetraethylorthosilicate (27.4 g, 131 mmol) was added dropwise to the aqueous solution for 2 h and magnetically stirred for further 19 h at room temperature and the

formed precipitate was collected by filtration. The obtained precipitate was washed with an ethanol solution (100 g) containing ammonium nitrate (500 mg, 6.25 mmol) at 60 °C, then, water and ethanol, successively. The precipitate was collected by filtration and dried at 200 °C. The obtained spherical MCM-41 was suspended to an aqueous solution (400 mL) of sodium aluminate (1.33 g, 21.7 mmol) and stirred for 22 h at room temperature. The obtained solid was collected by filtration and dried at 200 °C for 1 h. The dried sample was calcined at 550 °C for 6 h under atmospheric conditions to obtain sAl-MCM-41. The obtained powder was characterized by $N_2$ adsorption-desorption at 77 K and powder X-ray diffraction.

**Preparation of $[Fe(H_2O)_3]_2[Ru(CN)_6]$@sAl-MCM-41 and $[Cu(H_2O)_n]_2[Ru(CN)_6]$@sAl-MCM-41.** $[Fe(H_2O)_3]_2[Ru(CN)_6]$@sAl-MCM-41 and $[Cu(H_2O)_n]_2[Ru(CN)_6]$@sAl-MCM-41 were prepared by a similar procedure. sAl-MCM-41 (0.20 g) was added to an aqueous solution (10 mL) of iron(II) perchlorate hydrate (0.20 g, 0.56 mmol) or copper(II) sulfate pentahydrate (0.14 g, 0.56 mmol) and magnetically stirred for 2 h at room temperature. The obtained solid collected by centrifugation was washed with water two times and dried *in vacuo*. The obtained $Fe^{2+}$@sAl-MCM-41 or $Cu^{2+}$@sAl-MCM-41 (50 mg) was added to an aqueous solution of potassium hexacyanoruthenate(II) hydrate (57 mg, 0.14 mmol) for 2 h on a magnetic stirrer. The obtained solid was collected by filtration and washed with water and dried *in vacuo* to obtain $[Fe(H_2O)_3]_2[Ru(CN)_6]$@sAl-MCM-41 or $[Cu(H_2O)_n]_2[Ru(CN)_6]$@sAl-MCM-41. The loading amounts of Fe and Ru on the sAl-MCM-41 were determined by X-ray fluorescence (XRF) measurements to be $8.7 \times 10^{-4}$ and $5.7 \times 10^{-5}$ mol $g^{-1}$, respectively.[34]

**$N_2$ Adsorption-Desorption Isotherms.** Nitrogen adsorption-desorption isotherms at 77 K were recorded by an instrument for volumetric adsorption measurements, Belsorp-mini II (BEL Japan, Inc.), within a relative pressure range from 0.01 to 101.3 kPa. The mass of a sample was

ca. 100 mg for an adsorption analysis after pretreatment at 393 K for ca. 1 h under vacuum conditions and kept in $N_2$ atmosphere until $N_2$-adsorption measurements. The sample was exposed to a mixed gas of He and $N_2$ with a programmed ratio and adsorbed amount of $N_2$ was calculated from the change of pressure in a cell after reaching the equilibrium.

**Powder X-ray Diffraction.** Powder X-ray diffraction patterns were recorded on a Rigaku MiniFlex 600. Incident X-ray radiation was produced by a Cu X-ray tube operating at 40 kV and 15 mA with Cu K$\alpha$ radiation ($\lambda$□= 1.54 Å). The scan rate was 1° $min^{-1}$ from $2\theta$ = 2 – 40°.

**Physical Measurements.** UV-vis absorption spectra of solutions were recorded on a Hewlett Packard 8453 diode array spectrometer. UV-vis diffused reflectance spectra were measured by a Jasco V-670 spectrometer equipped with an SIN-768 attachment. IR spectra were recorded on a Jasco FT/IR-6200 spectrometer for the samples pelletized with KBr. The EPR spectra were taken on a JEOL X-band spectrometer (JES-REIXE) with a quartz EPR tube (4.5 mm) at 150 K. The *g* values were calibrated using an $Mn^{2+}$ marker. Sub-nanosecond laser-induced transient absorption spectra were collected by a customized measuring system equipped with a ps-pulse laser for the photoexcitation and a photomultiplier detector developed by UNISOKU Co., Ltd. Nanosecond laser flash photolysis experiments were performed using an Nd:YAG laser (Continuum, SLI-20, 4 – 6 ns fwhm) at $\lambda$ = 266 nm with the power of 0.5 mJ per pulse.[35] The transient absorption measurements were performed using a continuous wave xenon lamp (150 W) and a photomultiplier (Hamamatsu 2949) as a probe light and a detector, respectively. The output from a photomultiplier was recorded on a digitizing oscilloscope (Tektronix, TDS3032, 300 MHz). XRF measurements were performed to determine the loading amount of $[Fe(H_2O)_3]_2[Ru(CN)_6]$ on sAl-MCM-41 by a Rigaku ZSX-100e, which is a wavelength-dispersive spectrometer equipped with a 4 kW Rh X-ray tube.

**Hydroxylation of Benzene by $H_2O_2$.** Typical reaction conditions are as follows: $[Fe(H_2O)_3]_2[Ru(CN)_6]$@sAl-MCM-41 (1.0 mg, 17 μM of $[Fe(H_2O)_3]_2[Ru(CN)_6]$) was suspended to MeCN (2.5 mL). Benzene (0.40 mL, 1.4 M) and aqueous hydrogen peroxide (30 wt%; 0.40 mL, 1.2 M) was added to the suspension successively under vigorous stirring at 298 K. A small portion of the reaction solution was taken out and injected to a Shimadzu QP-5000 GC/MS to analyze products.

**Photocatalytic Production of $H_2O_2$.** Typical reaction conditions are as follows: $[Fe(H_2O)_3]_2[Ru(CN)_6]$@sAl-MCM-41 (1.0 mg, 17 μM of $[Fe(H_2O)_3]_2[Ru(CN)_6]$) was suspended to an $O_2$-saturated mixed solution (3.3 mL) composed of MeCN and water [2.9:0.40 (v/v)] containing $Sc(NO_3)_3$ (0.10 M). The suspension was gently stirred by a magnetic stirrer under photoirradiation with a xenon lamp (Ushio Optical, Model X SX-UID 500X AMQ) at room temperature. The amount of produced $H_2O_2$ at each reaction time was determined by the titration of iodide ion. The photocatalytic production of $H_2O_2$ was also performed in $^{16}O_2$-saturated $H_2{}^{18}O$ containing $[Fe(H_2O)_3]_2[Ru(CN)_6]$. After removal of $^{16}O_2$ and $^{18}O_2$ in the gas phase by passing He gas, the reaction solution was moved to a sealed vial containing $MnO_2$, which catalyzes $H_2O_2$ decomposition, via cannula under He atmosphere. The evolved oxygen gas in the headspace was analyzed by a gas chromatograph [He carrier, TC-FFAP column (GL Science, 1010-15242) at 313 K] equipped with a mass spectrometer (Shimadzu, QP-5000 GC/MS).

**Photocatalytic Water Oxidation.** Typical reaction conditions are as follows: a heteropolynuclear cyanide complex (0.54 mM) was suspended to an Ar-saturated phosphate buffer (50 mM, pH 8.0, 2.0 mL) containing $Na_2S_2O_8$ (10 mM) and $[Ru(bpy)_3]Cl_2$ (1.0 mM). The solution was then irradiated with the xenon lamp through a color filter glass (Asahi Techno Glass) transmitting $\lambda > 390$ nm at room temperature. The concentration of oxygen gas in a

headspace was quantified by a Shimadzu GC-17A gas chromatograph [Ar carrier, a capillary column with molecular sieves (Agilent Technologies, 19095PMS0, 30 m × 0.53 mm) at 313 K] equipped with a thermal conductivity detector (TCD) at a certain reaction time.

**Thermal Water Oxidation.** $[Ru^{III}(bpy)_3](PF_6)_3$ (0.50 mM) and $[Fe(H_2O)_3]_2[Ru(CN)_6]$ (1.0 mg) were dissolved to a phosphate buffer (2.0 mL, 50 mM, pH 8.0) in a sealed vial under Ar atmosphere. After a certain reaction time, the concentration of oxygen gas in the headspace of the reaction vial was quantified by a gas chromatograph with a TCD.

**$^{18}$O-Isotope Labeling Experiments.** $[Fe(H_2O)_3]_2[Ru(CN)_6]$ (5.0 mg, 6.8 mM) was suspended to an He-saturated $H_2{}^{18}O$ (2.0 mL) containing $Na_2S_2O_8$ (10 mM) and $[Ru(bpy)_3]Cl_2$ (1.0 mM). The suspension was then irradiated with a xenon lamp ($\lambda$ > 390 nm) at room temperature. The concentration of oxygen gas in a headspace was quantified by a gas chromatograph equipped with a mass spectrometer (Shimadzu, QP-5000 GC/MS).

**Hydroxylation of Benzene with $O_2$.** Typical reaction conditions are as follows: $[Fe(H_2O)_3]_2[Ru(CN)_6]$@sAl-MCM-41 (1.0 mg, 17 μM of $[Fe(H_2O)_3]_2[Ru(CN)_6]$) was suspended to an $O_2$-saturated mixed solution (3.3 mL) composed of MeCN and benzene [2.9 : 0.40 (v/v)]. The suspension was magnetically stirred under photoirradiation at room temperature. Product analyses were performed by a Shimadzu QP-5000 GC/MS.

## Results and Discussion

**Catalytic Hydroxylation of Benzene by $H_2O_2$ Using $[Fe(H_2O)_3]_2[Ru(CN)_6]$@sAl-MCM-41.** Nanosized spherical mesoporous silica-alumina (sAl-MCM-41), which is highly dispersible to a

solvent and can efficiently prevent the growth of $[Fe(H_2O)_3]_2[Ru(CN)_6]$ particles in mesopores, was synthesized by using a mixture of tetraethyl orthosilicate and sodium aluminate as precursors under basic (aqueous $NH_3$) conditions.[33] The addition of $Al^{3+}$ to silica results in formation of cation-exchange sites, which are important to enhance interaction between metal ions and the surfaces. The Brunauer-Emmett-Teller (BET) surface area of sAl-MCM-41 was determined to be 758 $m^2\ g^{-1}$ based on the $N_2$ adsorption-desorption isotherms [Figure S1a in Supporting Information (SI)]. The powder XRD pattern of sAl-MCM-41 indicates that the pore diameter is 3.7 nm, which is the same value determined by the Barrett-Joyner-Halenda (BJH) pore size distribution (Figures S1b and S2 in SI). $[Fe(H_2O)_3]_2[Ru(CN)_6]$ was incorporated in sAl-MCM-41 by the reaction of $Fe^{2+}$ adsorbed on sAl-MCM-41 and $K_4[Ru^{II}(CN)_6]$ ($[Fe(H_2O)_3]_2[Ru(CN)_6]$@sAl-MCM-41) in water. When sAl-MCM-41 without loading $Fe^{2+}$ was used instead of the $Fe^{2+}$ adsorbed sAlMCM-41, no incorporation of $[Ru^{II}(CN)_6]^{4-}$ was observed (Figure S3 in SI). The formation and incorporation of $[Fe(H_2O)_3]_2[Ru(CN)_6]$ was confirmed by a diffuse reflectance UV-vis absorption spectrum, powder X-ray diffraction and TEM images with elemental mappings of Ru and Fe as shown in Figures S4 and S5 in SI, where the absorption band and diffraction patterns due to $[Fe(H_2O)_3]_2[Ru(CN)_6]$ were observed. The amount of incorporated $[Fe(H_2O)_3]_2[Ru(CN)_6]$ was determined to be $5.7 \times 10^{-5}$ mol $g^{-1}$, which corresponds to 2.1% of the cation exchange sites of sAl-MCM-41, by X-ray fluorescent measurements. The BET surface area and pore volume of $[Fe(H_2O)_3]_2[Ru(CN)_6]$@sAl-MCM-41 were determined to be 526 $m^2\ g^{-1}$ and 0.439 $cm^3\ g^{-1}$, respectively, which are lower than those of bare sAl-MCM-41 (758 $m^2\ g^{-1}$ and 0.491 $cm^3\ g^{-1}$) (Figure S6 in SI). The lower BET surface area mainly resulted from the decrease of the inner surface area to 478 from 708 $m^2\ g^{-1}$. No significant change in the

BJH pore size distribution for both samples suggested that $[Fe(H_2O)_3]_2[Ru(CN)_6]$ mainly located inside mesopores and partly filled them.

Firstly, catalytic hydroxylation of benzene (0.40 mL, 1.4 M) by 30 wt% aqueous $H_2O_2$ (0.40 mL, 1.2 M) to produce phenol was examined by using $[M(H_2O)_3]_2[Ru(CN)_6]$ without sAl-MCM-41 (0.10 mg, 82 μM; M = Mn, Fe, Co or Cu) as a heterogeneous catalyst in MeCN (2.5 mL) (Figure 2). Among the catalysts, $[Fe(H_2O)_3]_2[Ru(CN)_6]$ showed the highest reactivity in terms of

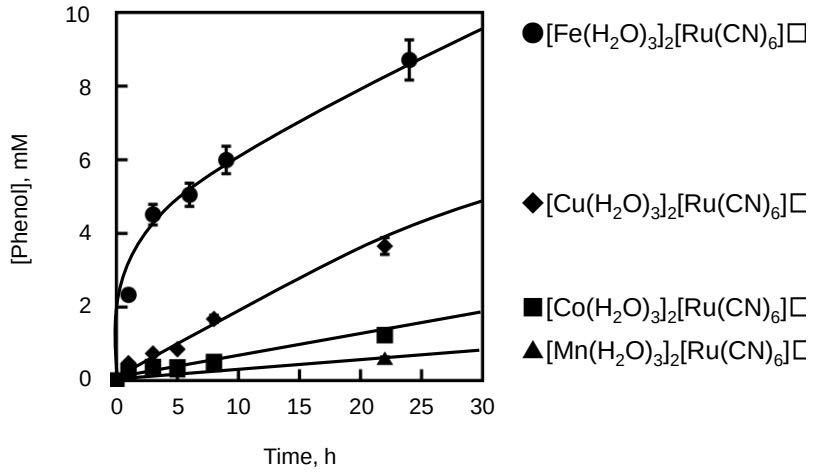


**Figure 2.** Time profiles of production of phenol in catalytic hydroxylation of benzene (0.40 mL, 1.4 M) with 30 wt% aqueous $H_2O_2$ (0.40 mL, 1.2 M) in MeCN (2.5 mL) containing $[M(H_2O)_3]_2[Ru(CN)_6]$ (M = Mn, Fe, Co or Cu) (0.10 mg , 82 μM) at 323 K.

a yield and a rate of phenol production. The apparent turnover number (TON) of phenol production per the monomer unit of $[Fe(H_2O)_3]_2[Ru(CN)_6]$ was 393 at 60 h. The over-oxidation products such as *p*-benzoquinone were not produced and the product selectivity to phenol was >99% (Figure 3). When the concentration of benzene was decreased to 4.3 mM, the yield of

phenol increased to 15% with >99% selectivity. No further oxidation of phenol to *p*-benzoquinone occurred at 323 K when the conversion of benzene was lower than 15%. The high selectivity to phenol may result from the interaction of formed phenol with Lewis acid sites,

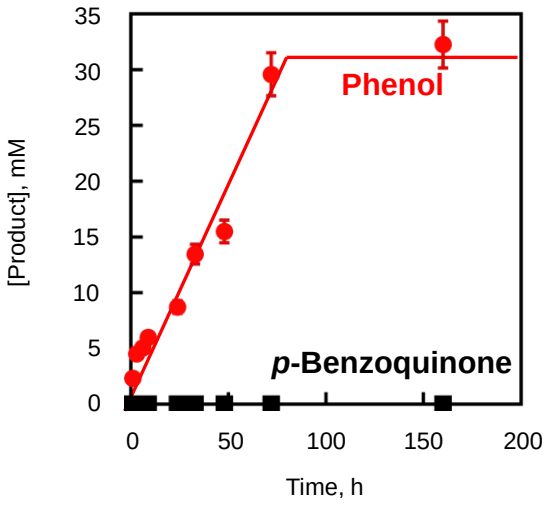


**Figure 3.** Time profiles of production of phenol (red circle) and *p*-benzoquinone (black square) in catalytic hydroxylation of benzene (0.40 mL, 1.5 M) with aqueous $H_2O_2$ (0.40 mL, 1.3 M) in MeCN (2.5 mL) containing $[Fe(H_2O)_3]_2[Ru(CN)_6]$ (0.10 mg , 82 μM) at 323 K.

which suppresses further oxidation.[6a,36-38] The initial rate of formation of phenol (< 2 h) was proportional to concentrations of benzene and $[Fe(H_2O)_3]_2[Ru(CN)_6]$, whereas the rate remains constant irrespective of different concentrations of $H_2O_2$ (see Figure S7 in SI). The first-order dependence of the rate on the catalyst concentration suggests that the monomer unit of $[Fe(H_2O)_3]_2[Ru(CN)_6]$ acts as the catalyst when no dissociation or association of $[Fe(H_2O)_3]_2[Ru(CN)_6]$ may be involved in the catalytic hydroxylation of benzene with $H_2O_2$. No dependence of the rate on concentration of $H_2O_2$ suggests that the catalyst forms a complex with $H_2O_2$ such as metal-peroxo or metal-oxo species during the catalytic reaction.

When $[Fe(H_2O)_3]_2[Ru(CN)_6]$@sAl-MCM-41 was employed as a catalyst, the apparent TON of phenol production per the monomer unit of incorporated $[Fe(H_2O)_3]_2[Ru(CN)_6]$ reached 2500 at 114 h (Figure 4). The incorporation of $[Fe(H_2O)_3]_2[Ru(CN)_6]$ in sAl-MCM-41 resulted in significant improvement of the catalytic durability by increasing the number of true active sites.

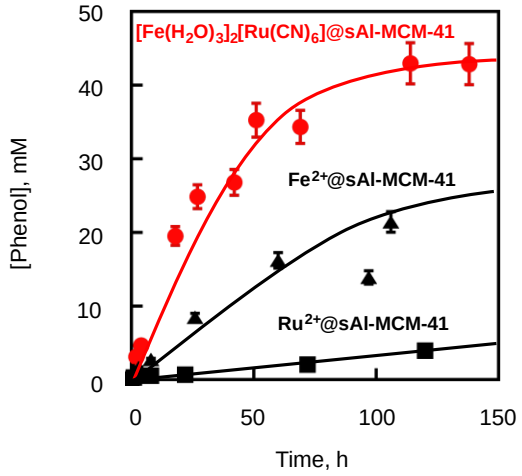


**Figure 4.** Time profiles of production of phenol in catalytic hydroxylation of benzene (0.40 mL, 1.5 M) with 30 wt% aqueous $H_2O_2$ (0.40 mL, 1.3 M) in MeCN (2.5 mL) containing $[Fe(H_2O)_3]_2[Ru(CN)_6]$@sAl-MCM-41 (1.0 mg, 17 μM of $[Fe(H_2O)_3]_2[Ru(CN)_6]$, red circle), $Fe^{2+}$@sAl-MCM-41 (1.0 mg, 34 μM of $Fe^{2+}$, black triangle) and $Ru^{2+}$@sAl-MCM-41 (2.3 mg, 17 μM of $Ru^{2+}$, black square) at 323 K.

During the reaction, 100 mM of $H_2O_2$ was consumed for producing 37 mM phenol, suggesting that the oxidation reaction accompanied with the decomposition of $H_2O_2$ by disproportionation as evidenced by tiny bubbles formation in the reaction vial. Lower apparent TONs were achieved by employing $Fe^{2+}$ or $Ru^{2+}$ incorporated in sAl-MCM-41 ($Fe^{2+}$@sAl-MCM-41 or $Ru^{2+}$@sAl-MCM-41) as a catalyst for benzene hydroxylation under the same reaction conditions for the

reaction system employing $[Fe(H_2O)_3]_2[Ru(CN)_6]$@sAl-MCM-41, suggesting that formation of $[Fe(H_2O)_3]_2[Ru(CN)_6]$ is important to exhibit high catalytic activity.

**Photocatalytic $H_2O_2$ Production from $H_2O$ and $O_2$ Using $[Fe(H_2O)_3]_2[Ru(CN)_6]$@sAl-MCM-41.** It was also found that $[Fe(H_2O)_3]_2[Ru(CN)_6]$@sAl-MCM-41 acted as an effective photocatalyst for production of $H_2O_2$ from $H_2O$ and $O_2$ by photoirradiation of an $O_2$-satuated aqueous dispersion containing $[Fe(H_2O)_3]_2[Ru(CN)_6]$@sAl-MCM-41 and $Sc(NO_3)_3$ as shown in Figure 5. The presence of $Sc^{3+}$ has been reported to stabilize $O_2^{\bullet-}$, which is converted to $H_2O_2$ and

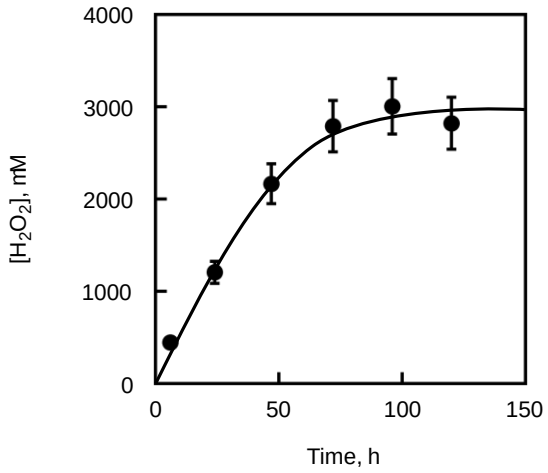


**Figure 5.** Time course of production of $H_2O_2$ from $H_2O$ and $O_2$ in an $O_2$-saturated MeCN (2.9 mL) containing $[Fe(H_2O)_3]_2[Ru(CN)_6]$@sAl-MCM-41 (1.0 mg, 17 μM of $[Fe(H_2O)_3]_2[Ru(CN)_6]$), water (0.40 mL) and $Sc(NO_3)_3$ (0.10 M) under photoirradiation with a xenon lamp.

$O_2$ by disproportionation.[25,26] The photocatalytic $H_2O_2$ formation was also performed by using $^{16}O_2$-saturated mixed solvent of MeCN and $H_2{}^{18}O$ [2.9:0.4 (v/v)] under the same reaction conditions other than the solvent. The formed $H_2O_2$, which was catalytically decomposed to $O_2$

by $MnO_2$ for analyses, contained only $^{16}O$, suggesting that $^{16}O_2$ is an electron acceptor in this reaction system (Figure S8). No $H_2O_2$ formation was observed when $[Cu(H_2O)_n]_2[Ru(CN)_6]$@sAl-MCM-41 or $K_4[Ru^{II}(CN)_6]$ was used instead of $[Fe(H_2O)_3]_2[Ru(CN)_6]$@sAl-MCM-41 in the reaction dispersion (Figure S9 in SI), indicating that the $Fe^{II}$ moiety is necessary to exhibit the catalysis for $H_2O_2$ production.

The role of $Fe^{II}$ moiety seemed to be an active site for water oxidation, because some cyano-bridged polynuclear metal complexes have been reported to act as water oxidation catalysts, in which N-bound metal ions are active sites.[39] Catalysis of $[Fe(H_2O)_3]_2[Ru(CN)_6]$ was examined for the photocatalytic water oxidation by $S_2O_8^{2-}$ in the presence of $[Ru^{II}(bpy)_3]^{2+}$ (bpy = 2, 2'-bipyridine) as a photosensitizer. Steady $O_2$ evolution was observed for 30 min under visible light irradiation ($\lambda$□> 390 nm) as shown in Figure 6. In a previous report, the intermediate $SO_4^{\bullet-}$ formed by one-electron oxidation of $S_2O_8^{2-}$ is a strong oxidant so that it may oxidize WOCs directly.[40] To exclude this possibility, $[Ru^{III}(bpy)_3]^{3+}$ thermally produced by oxidation of $[Ru^{II}(bpy)_3]^{2+}$ with $PbO_2$ was employed as an oxidant for water oxidation.[41] $O_2$ evolved from a phosphate buffer (pH 8.0) contained both $[Ru^{III}(bpy)_3]^{3+}$ and $[Fe(H_2O)_3]_2[Ru(CN)_6]$, whereas no $O_2$ evolved without $[Fe(H_2O)_3]_2[Ru(CN)_6]$ (Figure S10). Thus, the $[Ru^{III}(bpy)_3]^{3+}$ formed during the photocatalytic water oxidation can oxidize the WOC to evolve $O_2$.

Similarly, $[Fe(H_2O)_2]_{1.5}[Rh(CN)_6]$, which possesses the $Fe^{II}$ moiety without the $[Ru(CN)_6]$ moiety, exhibits catalytic activity for water oxidation when the reaction system employed $[Fe(H_2O)_2]_{1.5}[Rh(CN)_6]$, instead of $[Fe(H_2O)_3]_2[Ru(CN)_6]$ as the water oxidation catalyst. These results manifested that $Fe^{II}$ moiety act as a catalytic active site for water oxidation in the cyano-

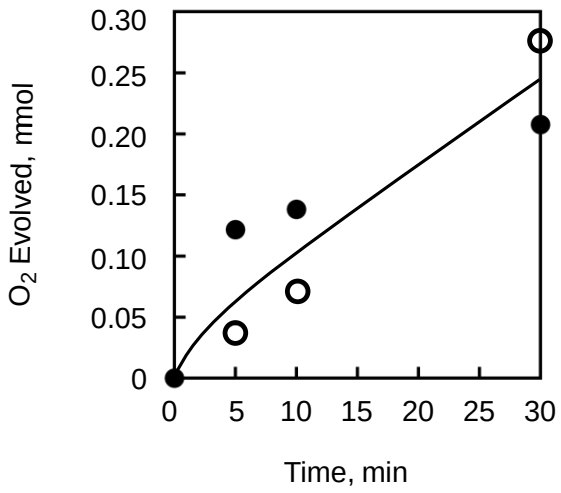


**Figure 6.** Time profiles of $O_2$ evolution under photoirradiation ($\lambda$□> 390 nm) of an Ar-saturated phosphate buffer (2.0 mL, 50 mM, pH 8.0) containing $Na_2S_2O_8$ (10 mM), $[Ru^{II}(bpy)_3]^{2+}$ (1.0 mM) and $[Fe(H_2O)_3]_2[Ru(CN)_6]$ (0.54 mM, closed circle) or $[Fe(H_2O)_2]_{1.5}[Rh(CN)_6]$ (0.54 mM, open circle).

bridged complexes.

$^{18}O$-isotope labeling experiments using $H_2{}^{18}O$ instead of $H_2{}^{16}O$ were conducted to obtain the direct evidence for the water oxidation. The evolved oxygen in the headspace of a vial after photoirradiation of a reaction suspension for a certain time was analyzed by a gas chromatograph equipped with a molecular sieve column and a mass spectrometer (Figure 7). The evolved gas after photoirradiation for 30 min contained $^{18}O^{18}O$ and $^{18}O^{16}O$ with the ratio of 60:40, whilst the amount of formed $^{16}O_2$ was under the detection limit of the mass spectrometer. The $^{16}O$ atom of $^{18}O^{16}O$ originates from water molecules of $[Fe(H_2{}^{16}O)_3]_2[Ru(CN)_6]$ contained as the extraligands.

Nanosecond laser-induced transient absorption spectra of $K_4[Ru^{II}(CN)_6]$ in water were measured to investigate a role of $[Ru^{II}(CN)_6]^{4-}$ moiety in the photocatalytic $H_2O_2$ formation

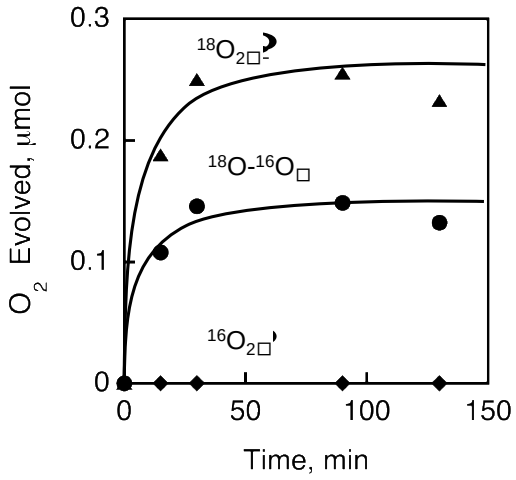


**Figure 7.** Time profiles of $^{16}O_2$ (◆), $^{18}O^{16}O$ (●) or $^{18}O_2$ (▲) evolution under photoirradiation ($\lambda$ > 390 nm) of a He-saturated $H_2{}^{18}O$ (2.0 mL) containing $Na_2S_2O_8$ (10 mM), $[Ru^{II}(bpy)_3]^{2+}$ (1.0 mM) and $[Fe(H_2O)_3]_2[Ru(CN)_6]$ (6.8 mM).

(Figure S11 in SI), where the absorption band at 750 nm is assigned to the excited state of $[Ru^{II}(CN)_6]^{4-}$ moiety. Transient absorption spectra of $[Fe(H_2O)_3]_2[Ru(CN)_6]$ also exhibited the absorption band at 750 nm (Figure S12 in SI). The lifetime of the excited state of $[Ru^{II}(CN)_6]^{4-}$ was determined to be 1.6 μs in deaerated MeCN. The lifetime of the excited state of $[Ru^{II}(CN)_6]^{4-}$ was shortened by increasing concentration of $O_2$ (Figure 8a). This suggests that electron transfer from the excited state of $[Ru^{II}(CN)_6]^{4-}$ to $O_2$ occurs to produce $[Ru^{III}(CN)_6]^{3-}$ and $O_2^{\bullet-}$. In the presence of $Sc^{3+}$ ions, $O_2^{\bullet-}$ is bound to a $Sc^{3+}$ ion to afford the $O_2^{\bullet-}$–$Sc^{3+}$ complex, which was detected by EPR after photoirradiation of an $O_2$-saturated MeCN solution of $[Fe(H_2O)_3]_2[Ru(CN)_6]$ at 150 K as shown in Figure 9, where the signal due to $[Ru^{III}(CN)_6]^{3-}$ was also observed (see reference spectra in Figure S13 in SI).[42] The rate constant of electron transfer from the excited state of $[Ru^{II}(CN)_6]^{4-}$ to $O_2$ was determined from the linear plot of the decay

rate constant vs concentration of $O_2$ (Figure 8b) to be $1.8 \times 10^{10}$ $M^{-1}$ $s^{-1}$, which is diffusion-limited.

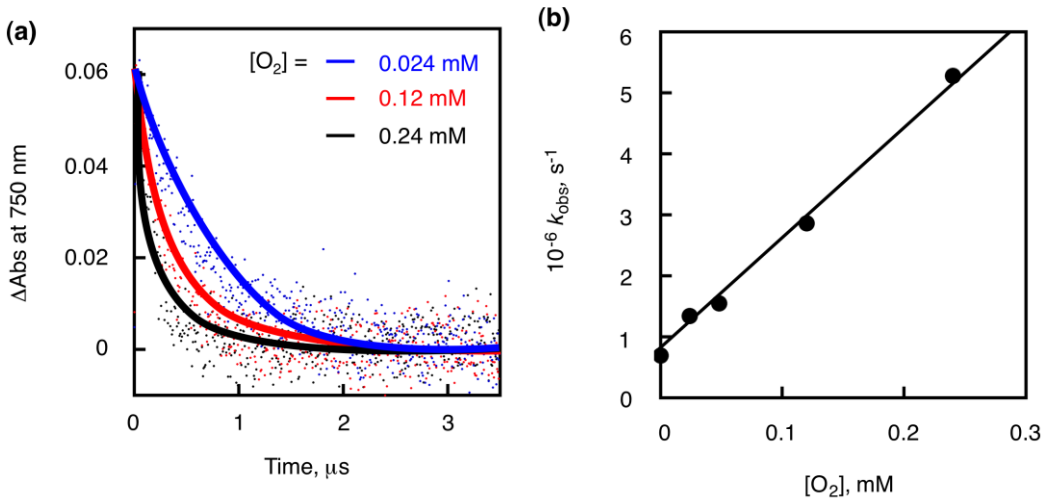


**Figure 8.** (a) Decay time profiles of absorbance at 750 nm observed in $N_2$-saturated MeCN containing $K_4[Ru^{II}(CN)_6]$ (1.8 mM) and various concentrations of $O_2$ (0-0.24 mM). (b) Plot of the decay rate constant vs concentration of $O_2$.

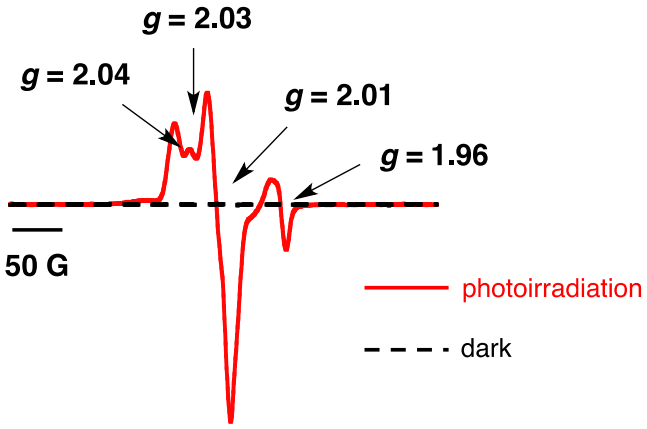

**Figure 9.** EPR spectra observed under dark (black broken line) and photoirradiation (red solid line) with an Hg lamp of an $O_2$-saturated MeCN solution (2.0 mL) containing $[Fe(H_2O)_3]_2[Ru(CN)_6]$ (0.20 mg, 0.27 mM) and $Sc(NO_3)_3$ (0.10 M) at 150 K.

The mechanism of the photocatalytic production of $H_2O_2$ from $H_2O$ and $O_2$ with $[Fe(H_2O)_3]_2[Ru(CN)_6]$@sAl-MCM-41 in MeCN is shown in Scheme 1. Photoexcitation of

**Scheme 1.** Overall Photocatalytic Cycle for $H_2O_2$ Production

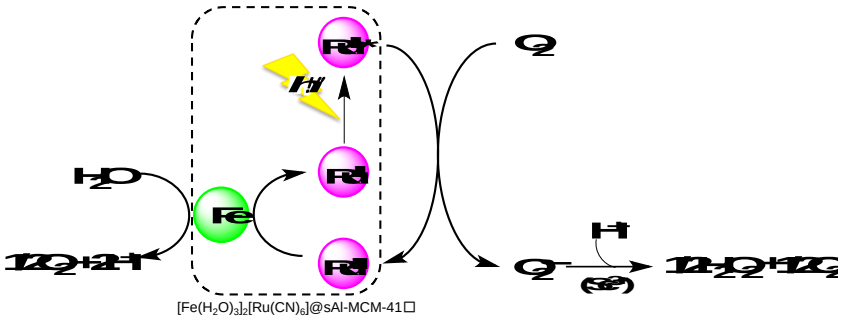


$[Fe(H_2O)_3]_2[Ru(CN)_6]$ resulted in electron transfer from the excited state of $[Fe(H_2O)_3]_2[Ru(CN)_6]$ to $O_2$ in the presence of $Sc^{3+}$ to produce $[Fe(H_2O)_3]_2[Ru^{III}(CN)_6]^+$ and $O_2^{\bullet-}$–$Sc^{3+}$. The reduction potential of $[Ru^{III}(CN)_6]^{3-}$ moiety in the presence of iron ions has been reported as $E_{1/2}$ = 1.24 V vs SHE,[43] which can oxidize the $Fe^{II}$ moiety to high-valent iron species suitable for water oxidation, because the standard electrode potential for water oxidation to evolve oxygen at the pH of the reaction solution (2.8) is 1.06 V vs SHE. The $O_2^{\bullet-}$–$Sc^{3+}$ complex disproportionates in the presence of $H^+$ to produce $H_2O_2$.[25,26]

**Photocatalytic Benzene Hydroxylation by $O_2$ Using $[Fe(H_2O)_3]_2[Ru(CN)_6]$@sAl-MCM-41.** The catalytic hydroxylation of benzene with $H_2O_2$ to phenol (eq 1) was combined with the photocatalysis of $[Fe(H_2O)_3]_2[Ru(CN)_6]$@sAl-MCM-41 for production of $H_2O_2$ from $H_2O$ and $O_2$ (eq 2). The overall catalytic reaction is given by eq 3, which shows the photocatalytic

$$C_6H_6 + H_2O_2 \xrightarrow[[Fe(H_2O)_3]_2[Ru(CN)_6]@sAl\text{-}MCM\text{-}41]{} C_6H_5OH + H_2O \quad (1)$$

$$H_2O + 1/2O_2 \xrightarrow[[Fe(H_2O)_3]_2[Ru(CN)_6]@sAl\text{-}MCM\text{-}41]{h\nu} H_2O_2 \quad (2)$$

$$C_6H_6 + 1/2O_2 \xrightarrow[[Fe(H_2O)_3]_2[Ru(CN)_6]@sAl\text{-}MCM\text{-}41]{h\nu} C_6H_5OH \quad (3)$$

hydroxylation of benzene to phenol using $O_2$ as an oxygen source as well as an oxidant. The time profile of production of phenol by photoirradiation of an $O_2$–saturated MeCN solution of benzene (0.40 mL, 1.5 M) containing $[Fe(H_2O)_3]_2[Ru(CN)_6]$@sAl-MCM-41 (1.0 mg, 17 μM of $[Fe(H_2O)_3]_2[Ru(CN)_6]$) at 298 K is shown in Figure 10. The TON reached 41 after photoirradiation for 59 h. Benzene hydroxylation to phenol was catalyzed by $[Fe(H_2O)_3]_2[Ru(CN)_6]$@sAl-MCM-41 with $H_2O_2$ even at a low concentration (3.0 mM) (Figure S14 in SI).

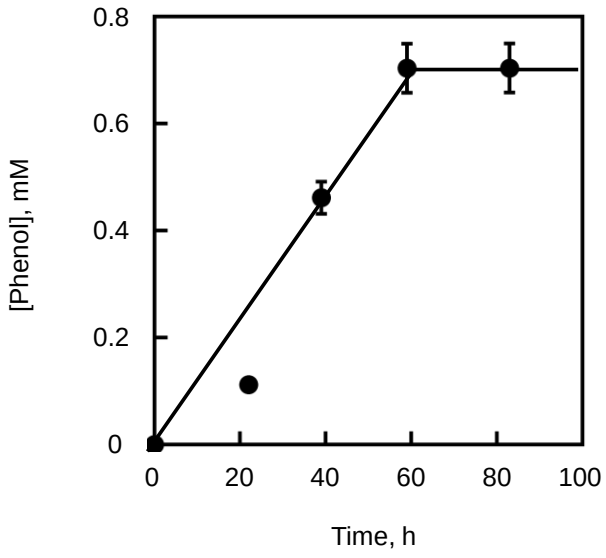

**Figure 10.** Time course of formation of phenol under photoirradiation of an $O_2$-saturated MeCN solution (2.9 mL) containing $[Fe(H_2O)_3]_2[Ru(CN)_6]$@sAl-MCM-41 (1.0 mg, 17 μM of $[Fe(H_2O)_3]_2[Ru(CN)_6]$) and benzene (1.5 M, 0.40 mL) with a xenon lamp.

## Conclusions

Hydroxylation of benzene to phenol has been achieved by using $O_2$ as an oxygen source as well as an oxidant by combination of the catalytic hydroxylation of benzene to phenol with $H_2O_2$ and the photocatalytic production of $H_2O_2$ from $H_2O$ and $O_2$ with use of $[Fe(H_2O)_3]_2[Ru(CN)_6]$@sAl-MCM-41, which acts as a catalyst for both benzene hydroxylation and water oxidation as well as a photocatalyst for $O_2$ reduction to $H_2O_2$. The combination of the catalytic hydroxylation of benzene to phenol with $H_2O_2$ and the photocatalytic production of $H_2O_2$ from $H_2O$ and $O_2$ in this study provides a new strategy to achieve one-pot hydroxylation of benzene with $O_2$ as an ideal oxygen source as well as an oxidant.

## ASSOCIATED CONTENT

**Supporting Information**. $N_2$-adsorption and desorption isotherms and BJH pore size distribution of sAl-MCM-41 and $[Fe(H_2O)_3]_2[Ru(CN)_6]$@sAl-MCM-41 (Figure S1 and S6), PXRD patterns (Figure S2 and S4b), UV-vis spectra (Figure S3 and S4a), TEM images with elemental mappings (Figure S5), time profiles of phenol production (Figure S7 and S14), distribution of $O_2$ in $^{18}O$-labelling experiment (Figure S8), time profiles of $H_2O_2$ production (Figure S9), time profiles of $O_2$ evolution (Figure S10), transient absorption spectra (Figure S11 and S12) and EPR spectra (Figure S13). This material is available free of charge via the Internet at http://pubs.acs.org.

AUTHOR INFORMATION

**Corresponding Author**

*E-mail: ymd@a-chem.eng.osaka-cu.ac.jp (Y.Y.), fukuzumi@chem.eng.osaka-u.ac.jp (S.F.).

**Author Contributions**

The manuscript was written through contributions of all authors. All authors have given approval to the final version of the manuscript.

**Funding Sources**

This work was supported by ALCA and SENTAN projects from JST (to S.F.) and JSPS KAKENHI (Nos. 24350069 and 15K14223 to Y.Y.).

**ACKNOWLEDGMENT**

We sincerely acknowledge Dr. Tatsuo Nakagawa and Mr. Kido Okamoto, Unisoku Co. Ltd., for the measurements of the laser-induced transient absorption spectra.

**REFERENCES**

(1) Sheldon, R. A.; van Santen, R. A. Catalytic Oxidation, Principles and Applications, World Scientific, Singapore, 1995.

(2) Panov, G. I. *CATTECH* **2000**, *4*, 18-32.

(3) Jiang, T.; Wang, W.; Han, B. *New J. Chem*. **2013**, *37*, 1654-1664.

(4) (a) Wen, G.; Wu, S.; Li, B.; Dai, C.; Su, D. S. *Angew. Chem., Int. Ed*. **2015**, *54*, 4105-4109. (b) Yang, J.-H.; Sun, G.; Gao, Y.; Zhao, H.; Tang, P.; Tan, J.; Lu, A.-H.; Ma, D. *Energy Environ. Sci*. **2013**, *6*, 793-798.

(5) (a) Shoji, O.; Kunimatsu, T.; Kawakami, N.; Watanabe, Y. *Angew. Chem., Int. Ed*. **2013**, *52*, 6606-6610. (b) Wang, X.; Zhang, T.; Yang, Q.; Jiang, S.; Li, B. *Eur. J. Inorg. Chem*. **2015**, 817‑825.

(6) (a) Aratani, Y.; Yamada, Y.; Fukuzumi, S. *Chem. Commun*. **2015**, *51*, 4662-4665. (b) Morimoto, Y.; Bunno, S.; Fujieda, N.; Sugimoto, H.; Itoh, S. *J. Am. Chem. Soc*. **2015**, *137*, 5867-5870. (c) Wu, L.; Zhong, W.; Xu, B.; Wei, Z.; Liu, X. *Dalton Trans*. **2015**, *44*, 8013-8020.

(7) (a) Wang, C.; Hu, L.; Hu, Y.; Ren, Y.; Chen, X.; Yue, B.; Heyong, H. *Catal. Commun*. **2015**, *68*, 1-5. (b) Fujishima, K.; Fukuoka, A.; Yamagishi, A.; Inagaki, S.; Fukushima, Y.; Ichikawa M. *J. Mol. Catal. A: Chem.* **2001**, *166*, 211-218.

(8) (a) Li, Y.; Feng, Z.; van Santena, R. A.; Hensen, E. J. M.; Li, C. *J. Catal*. **2008**, *255*, 190-196. (b) Koekkoek, A. J. J.; Degirmenci, V.; Hensen, E. J. M. *J. Mater. Chem*. **2011**, *21*, 9279-9289. (c) Koekkoek, A. J. J.; Kim, W.; Degirmenci, V.; Xin, H.; Ryoo, R.; Hensen, E. J. M. *J. Catal*. **2013**, *299*, 81-89. (d) Navarro, R.; Lopez-Pedrajas, S.; Luna, D.; Marinas, J. M.; Bautista, F. M. *Appl. Catal., A* **2014**, *474*, 272-279.

(9) (a) Ye, X.; Cui, Y.; Qiu, X.; Wang, X. *Appl. Catal., B: Environ*. **2014**, *152-153*, 383-389. (b) Notte, P. P. *Top. Catal*. **2000**, *13*, 387-394. (c) Yang, Z.; Yang, G.; Liu, X.; Han, X. *Catal. Lett*. **2013**, *143*, 260-266.

(10) (a) Niwa, S.; Eswaramoorthy, M.; Nair, J.; Raj, A.; Itoh, N.; Shoji, H.; Namba, T.; Mizukami, F. *Science* **2002**, *295*, 105-107. (b) Wang, X.; Meng, B.; Tan, X.; Zhang, X.; Zhuang, S.; Liu, L. *Ind. Eng. Chem. Res*. **2014**, *53*, 5636-5645.

(11) (a) Shang, S.; Chen, B.; Wang, L.; Dai, W.; Zhang, Y.; Gao, S. *RSC Adv*. **2015**, *5*, 31965-31971. (b) Long, Z.; Zhou, Y.; Chen, G.; Zhao, P.; Wang, J. *Chem. Eng. J*. **2014**, *239*, 19-25. (c) Long, Z.; Zhou, Y.; Ge, W.; Chen, G.; Xie, J.; Wang, Q.; Wang, J. *ChemPlusChem* **2014**, *79*, 1590-1596.

(12) (a) Remias, J. E.; Pavlosky, T. A.; Sen, A. *J. Mol. Catal. A: Chem.* **2003**, *203*, 179-192. (b) Kunai, A.; Kitano, T.; Kuroda, Y.; Lifen, J.; Sasaki, K. *Catal. Lett.* **1990**, *4*, 139-144.

(c) Miyake, T.; Hamada, M.; Sasaki, Y.; Oguri, M. *Appl. Catal., A* **1995**, *131*, 33-42. (d) Kitano, T.; Wani, T.; Ohnishi, T.; Lifen, J.; Kuroda, Y.; Kunai, A.; Sasaki, K. *Catal. Lett.* **1991**, *11*, 11-18.

(13) (a) Kitano, T.; Kuroda, Y.; Mori, M.; Ito, S.; Sasaki, K.; Nitta, M. *J. Chem. Soc. Perkin Trans. 2* **1993**, 981-985. (b) Ehrich, H.; Berndt, H.; Pohl, M. M.; Jahnisch, K.; Baerns, M. *Appl. Catal., A* **2002**, *230*, 271-280.

(14) (a) Tatsumi, T.; Yuasa, K.; Tominaga, H. *J. Chem. Soc., Chem. Commun.* **1992**, 1446–1447. (b) Wang, X. B.; Zhang, X. F.; Liu, H. O.; Qiu, J. S.; Han, W.; Yeung, K. L. *Catal. Today* **2012**, *193*, 151–157.

(15) (a) Laufer, W.; Niederer, J. P. M.; Hoelderich, W. F. *Adv. Synth. Catal.* **2002**, *344*, 1084-1089. (b) Laufer, W.; Hoelderich, W. F. *Chem. Commun.* **2002**, 1684-1685.

(16) (a) Acharyya, S. S.; Ghosh, S.; Tiwari, R.; Pendem, C.; Sasaki, T.; Bal, R. *ACS Catal*. **2015**, *5*, 2850-2858. (b) Bal, R.; Tada, M.; Sasaki, T.; Iwasawa, Y. *Angew. Chem., Int. Ed*. **2006**, *45*, 448-452.

(17) (a) Tada, M.; Uemura, Y.; Bal, R.; Inada, Y.; Nomura, M.; Iwasawa, Y. *Phys. Chem. Chem. Phys*. **2010**, *12*, 5701-5706. (b) Tada, M.; Bal, R.; Sasaki, T.; Uemura, Y.; Inada, Y.; Tanaka, S.; Nomura, M.; Iwasawa, Y. *J. Phys. Chem. C* **2007**, *111*, 10095-10104.

(18) (a) Long, Z.; Liu, Y.; Zhao, P.; Wang, Q.; Zhou, Y.; Wang, J. *Catal. Commun*. **2015**, *59*, 1-4. (b) Tablera, A.; Häussera, A.; Roduner, E. *J. Mol. Catal. A: Chem.* **2013**, *379*, 139-145. (c) Hamada, R.; Shibata, Y.; Nishiyama, S.; Tsuruya, S. *Phys. Chem. Chem. Phys*. **2003**, *5*, 956‑965.

(19) Guo, H.; Chen, Z.; Mei, F.; Zhu, D.; Xiong, H.; Yin, G. *Chem.–Asian J*. **2013**, *8*, 888-891.

(20) (a) Bui, T. D.; Kimura, A.; Ikeda, S.; Matsumura, M. *J. Am. Chem. Soc*. **2010**, *132*, 8453-8458. (b) Ide, Y.; Torii, M.; Sano, T. *J. Am. Chem. Soc*. **2013**, *135*, 11784-11786.

(21) (a) Fukuzumi, S.; Ohkubo, K. *Chem. Sci*. **2013**, *4*, 561-574. (b) Fukuzumi, S.; Ohkubo, K. *Org. Biomol. Chem*. **2014**, *12*, 6059-6071.

(22) Ohkubo, K.; Kobayashi, T.; Fukuzumi, S. *Angew. Chem., Int. Ed*. **2011**, *50*, 8652-8655.

(23) (a) Ohkubo, K.; Fujimoto, A.; Fukuzumi, S. *J. Am. Chem. Soc*. **2013**, *135*, 5368-5371. (b) Ohkubo, K.; Hirose, H.; Fukuzumi, S. *Chem.–Eur. J*. **2015**, *21*, 2855-2861.

(24) Kato, S.; Jung, J.; Suenobu, T.; Fukuzumi, S. *Energy Environ. Sci*. **2013**, *6*, 3756-3764.

(25) Isaka, Y.; Kato, S.; Hong, D.; Suenobu, T.; Yamada, Y.; Fukuzumi, S. *J. Mater. Chem. A* **2015**, *3*, 12404-12412.

(26) Isaka, Y.; Oyama, K.; Yamada, Y.; Suenobu, T.; Fukuzumi, S. *Catal. Sci. Technol.* **2016**, *6*, 681-684.

(27) Yamaguchi, S.; Ohnishi, T.; Miyake, Y.; Yahiro, H. *Chem. Lett.* **2015**, *44*, 1287-1288.

(28) Shul'pina, L. S.; Kudinov, A. R.; Mandelli, D.; Carvalho, W. A.; Kozlov, Y. N.; Vinogradov, M. M.; Ikonnikov, N. S.; Shul'pin, G. B. *J. Organomet. Chem.* **2015**, *793*, 217-231.

(29) Fukuzumi, S.; Ohkubo, K. *Asian J. Org. Chem.* **2015**, *4*, 836-845.

(30) (a) Kejriwal, A.; Bandyopadhyay, P.; Biswas, A. N. *Dalton Trans.* **2015**, *44*, 17261-17267. (b) Wang, X.; Zhang, T. Y.; Li, B.; Yang, Q. S.; Jiang, S. *Appl. Organomet. Chem.* **2014**, *28*, 666-672.

(31) (a) Chen, X. F.; Zhang, J. S.; Fu, X. Z.; Antonietti, M.; Wang, X. C. *J. Am. Chem. Soc.* **2009**, *131*, 11658-11659. (b) Bianchi, D.; Bortolo, R.; Tassinari, R.; Ricci, M.; Vignola, R. *Angew. Chem., Int. Ed.* **2000**, *39*, 4321-4323. (c) Wang, D.; Wang, M.; Li, Z. *ACS Catal.* **2015**, *5*, 6852-6857.

(32) Yamada, Y.; Yoneda, M.; Fukuzumi, S. *Chem.–Eur. J*. **2013**, *19*, 11733-11741.

(33) (a) Szegedi, Á.; Kónya, Z.; Méhn, D.; Solymár, E.; Pál-Borbély, G.; Horváth, Z. E.; Biró, L. P.; Kiricsi, I. *Appl. Catal., A* **2004**, *272*, 257-266. (b) Anunziata, O. A.; Martínez, M. L.; Costa, M. G. *Mater. Lett.* **2010**, *64*, 545-548.

(34) (a) Sharma, R. K.; Dutta, S.; Sharma, S. *Dalton Trans.* **2015**, *44*, 1303-1316. (b) Pérez, Y.; del Hierro, I.; Zazo, L.; Fernández-Galánb, R.; Fajardo, M. *Dalton Trans.* **2015**, *44*, 4088-4101. (c) De Decker, J.; Bogaerts, T.; Muylaert, I.; Delahaye, S.; Lynen, F.; Van Speybroeck, V.; Verberckmoes, A.; Van Der Voort, P. *Mater. Chem. Phys.* **2013**, *141*, 967-972.

(35) Kawashima, T.; Ohkubo, K.; Fukuzumi, S. *Org. Biomol. Chem*. **2010**, *8*, 994-996.

(36) (a) Olah, G. A.; White, A. M.; O'Brien, D. H. *Chem. Rev*. **1970**, *70*, 561-591. (b) Solcà N.; Dopfer, O. *Chem. Phys. Lett*. **2001**, *342*, 191-199.

(37) (a) Parker, W. O., Jr.; Wegner, S. *Microporous Mesoporous Mater*. **2012**, *158*, 235-240. (b) Gupta, P.; Paul, S. *Catal. Today* **2014**, *236*, 153-170.

(38) Guo, H.; Chen, Z.; Mei, F.; Zhu, D.; Xiong, H.; Yin, G. *Chem. Asian J.* **2013**, *8*, 888-891.

(39) (a) Yamada, Y.; Oyama, K.; Gates, R.; Fukuzumi, S. *Angew. Chem. Int. Ed.* **2015**, *54*, 5613-5617. (b) Goberna-Ferrón, S.; Hernández, W. Y.; Rodríguez-García, B.; Galán-Mascarós, J. R. *ACS Catal.* **2014**, *4*, 1637-1641. (c) Pintado, S.; Goberna-Ferron, S.; Escudero-Adan, E. C.; Galan-Mascaros, J. R. *J. Am. Chem. Soc.* **2013**, *135*, 13270-13273.

(40) Panda, C.; Debgupta, J.; Díaz, D. D.; Singh, K. K.; Gupta, S. S.; Dhar, B. B. *J. Am. Chem. Soc.* **2014**, *136*, 12273-12282.

(41) Kaveevivitchai, N.; Chitta, R.; Zong, R.; El Ojaimi, M.; Thummel, R. P. *J. Am. Chem. Soc.* **2012**, *134*, 10721-10724.

(42) Ritzert, N. L.; Rodríguez-López, J.; Tan, C.; Abruña, H. D. *Langmuir* **2013**, *29*, 1683-1694.

(43) Sone, K.; Yagi, M. *Macromol. Symp.* **2006**, *235*, 179-186.

**SYNOPSIS:** Combination of photo- and thermal catalysis of $Ru^{II}$ and $Fe^{II}$ in $[Fe(H_2O)_3]_2[Ru(CN)_6]$@sAl-MCM-41 enables photocatalytic benzene hydroxylation using molecular oxygen.

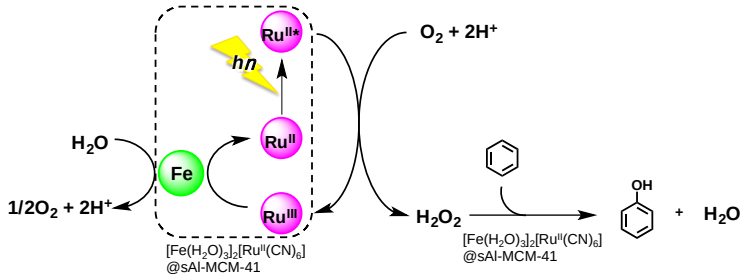


**Combination of photo- and thermal catalysis of $[Fe(H_2O)_3]_2[Ru(CN)_6]$ on sAl-MCM-41**